Hindawi
International Journal of Antennas and Propagation
Volume 2022, Article ID 8456936, 11 pages
https://doi.org/10.1155/2022/8456936

Research Article

A Wideband Eight-Element MIMO Antenna Array in 5G NR n77/78/79 and WLAN-5GHz Bands for 5G Smartphone Applications

Jun-Yi Jiang and Hsin-Lung Su

Department of Computer and Communication, National Pingtung University, Pingtung 900392, Taiwan

Correspondence should be addressed to Hsin-Lung Su; hlsu@mail.nptu.edu.tw

Received 19 August 2022; Accepted 5 October 2022; Published 16 November 2022

Academic Editor: Chow-Yen-Desmond Sim

In this paper, a wideband eight-element multiple-input multiple-output (MIMO) antenna array for 5G smartphone applications is presented. Each antenna is composed of a dual-arm tortuous monopole radiating element with a double-stub tuner and an open slot on the ground plane. Tuning stub microstrip lines are utilized to improve impedance matching. The operating bandwidth of the single antenna element is from 3200 to 6000 MHz with three resonant frequencies. The operating bandwidth covers the 5G new radio (NR) bands (n77/n78/n79) and the WLAN-5GHz band. The isolation of the proposed MIMO antenna array is above 10 dB in the entire operating band without any isolation elements. Furthermore, the proposed MIMO array was manufactured and measured. The measured results validate that the MIMO antenna array has a wide 6-dB impedance bandwidth from 3.2 to 6 GHz and the isolations are all more than 10 dB. The total efficiency ranges from 38% to 83%. The above results show that this MIMO antenna array can support 5G applications in smartphones.

1. Introduction

In recent years, people have pursued higher access rates and lower latency in the wireless network experience. Because the 4G LTE is no longer satisfied with current users, the 5G NR is proposed and rapidly expanding. The 3rd Generation Partnership Project (3GPP) has released some frequency bands, named n77 (3300–4200 MHz), n78 (3300–3800 MHz), and n79 (4400–5000 MHz) in its new specification for 5G NR. However, different countries have their own 5G frequency bands, but the selected frequency bands are always within those three mentioned frequency bands. Therefore, it is a good approach to design a wideband antenna that covers all 5G NR bands to comply with the specifications in the different countries.

MIMO technology is adopted to improve the access rate of mobile devices. The MIMO technology is widely used in 5G communication, and the access rate has been significantly improved by increasing the number of antenna array elements at the transmitting and receiving ends. It is easier to increase the number of antennas on the base station but is not in the smartphone. Because of the limited volume size of the smartphone, it is not easy to achieve high isolation of adjacent antennas without using any isolation elements and increasing the number of antennas simultaneously.

Some literature shows that the antenna itself is small but the distances between adjacent antennas are not close. Therefore, the isolation can reach more than 10 dB [1–8]. Some common techniques such as the neutralization line [9–11], self-isolated [12], polarization diversity [13], and decoupling by adding parasitic branches [9] or slots [14, 15] have been proposed and applied. Until now, many MIMO antenna array designs have been reported [1–16], and most of these papers proposed between 8 and 12 antenna elements array. It is not easy to obtain a wide-frequency bandwidth antenna with only one resonant mode to cover all 5G NR bands. Several articles have presented wideband antennas using multiple resonant modes [4–8, 15, 16]. For example, some papers present a wideband antenna composed of several individual elements which generated multiple and close resonant frequencies [4, 5, 7, 8]. In [6], this article presents a wideband loop antenna with creates a new

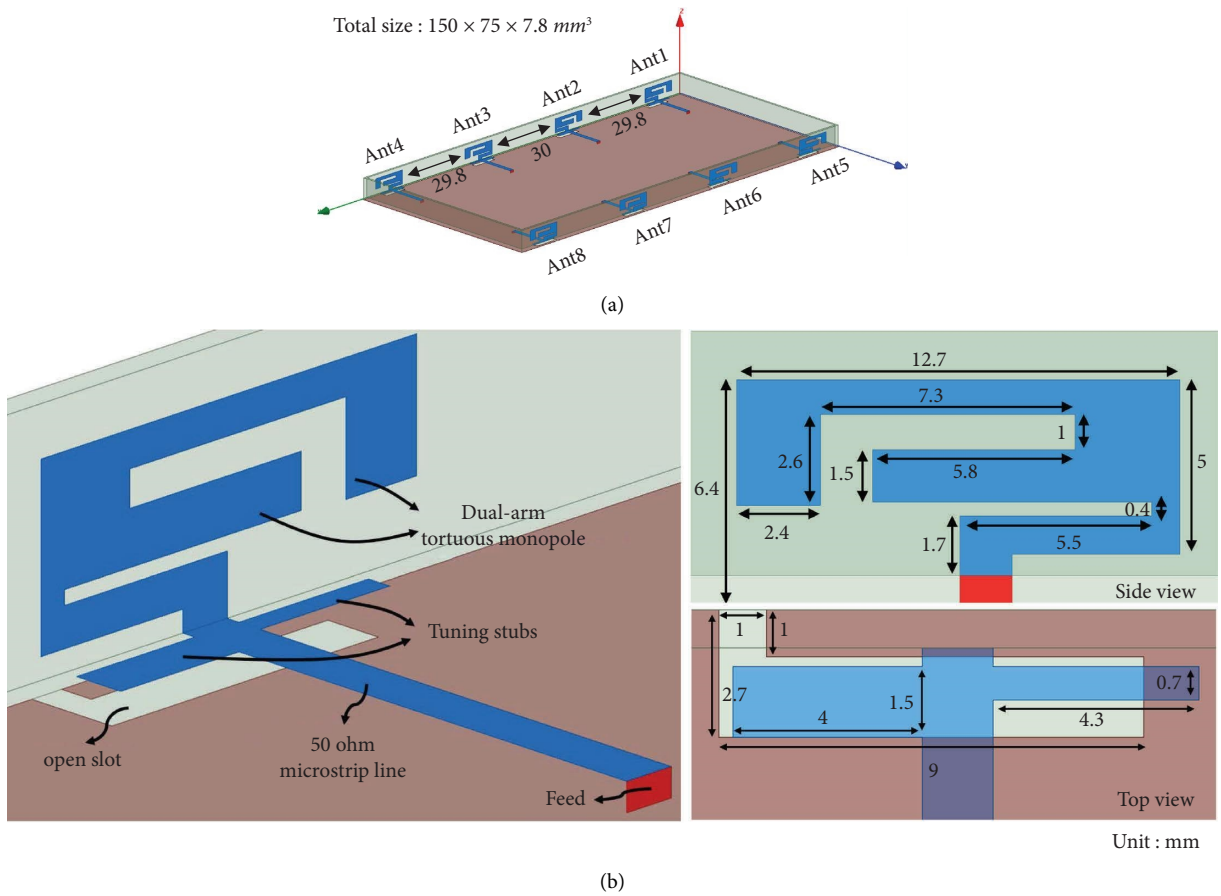

Figure 1: (a) The configuration of the MIMO antenna array and (b) the detailed parameters of the single antenna element.

resonant mode between the fundamental mode and the second harmonic mode. Therefore, this antenna creates three resonant modes which are 0.5 λ, 0.75 λ, and 1.0 λ, respectively, to obtain a wide frequency band. Creating different current paths on a single antenna element generates different resonant modes, such as the PIFA mode, the loop mode, and the slot mode, to compose a wide frequency band [16]. Most of the above studies fully cover the 5G NR bands (n77/n78/n79) and agree with the specification of 5G communications in different countries.

This article presents a wideband eight-element MIMO array with a simple structure for 5G NR smartphone applications. A dual-arm tortuous monopole antenna with an open slot to obtain a wide frequency bandwidth ranging from 3.3 to 5.95 GHz covers the 5G NR frequency bands and the WLAN-5 GHz band. The MIMO antenna array has isolation over 10 dB and is without any isolation elements or techniques.

2. Antenna Geometry and Design Steps

2.1. The Geometry of the Single Antenna Element. As shown in Figure 1(a), an eight-element antenna array is printed on the inner surface of two side edges of the smartphone with $150 \times 75 \times 7.8\,mm^3$. The antenna array is designed on a 0.8 mm thick FR4 substrate (relative permittivity 4.4 and loss tangent 0.02). The ground plane is installed on the bottom side of the smartphone substrate. The geometry and detail parameters of the single antenna element are depicted in Figure 1(b). The single antenna element includes two major parts, a dual-arm tortuous monopole element and an open slot on the ground plane, as shown in Figure 1(b). The single antenna element is fed by a 50 Ω microstrip line and the three-dimensional size of the proposed single antenna is $12.7 \times 6.4 \times 2.7\,mm^3$. The distances of each antenna are also depicted in Figure 1(a).

2.2. Design Steps of the Proposed Antenna Element. The design steps of this antenna and its corresponding S parameters are shown in Figure 2. Reference antenna 1 (Ref. 1) in Figure 2(a) is a tortuous monopole structure fed by a 50 Ω microstrip line, and it has one resonant frequency at approximately 3.8 GHz as the blue line shown in Figure 2(b). Worse impedance matching can be observed on the resonant frequency excited by the tortuous monopole structure. Therefore, Ref. 1 with loading a double-stub tuner on the feeding line to improve impedance matching, which forms reference antenna 2 (Ref. 2). The impedance matching of the resonant frequency at 3.8 GHz of Ref. 2 is greatly improved as the green line shown in Figure 2(b). Next, a dual-arm monopole structure is proposed in reference antenna 3 (Ref. 3) by etching an inverted-L slot on the tortuous monopole in

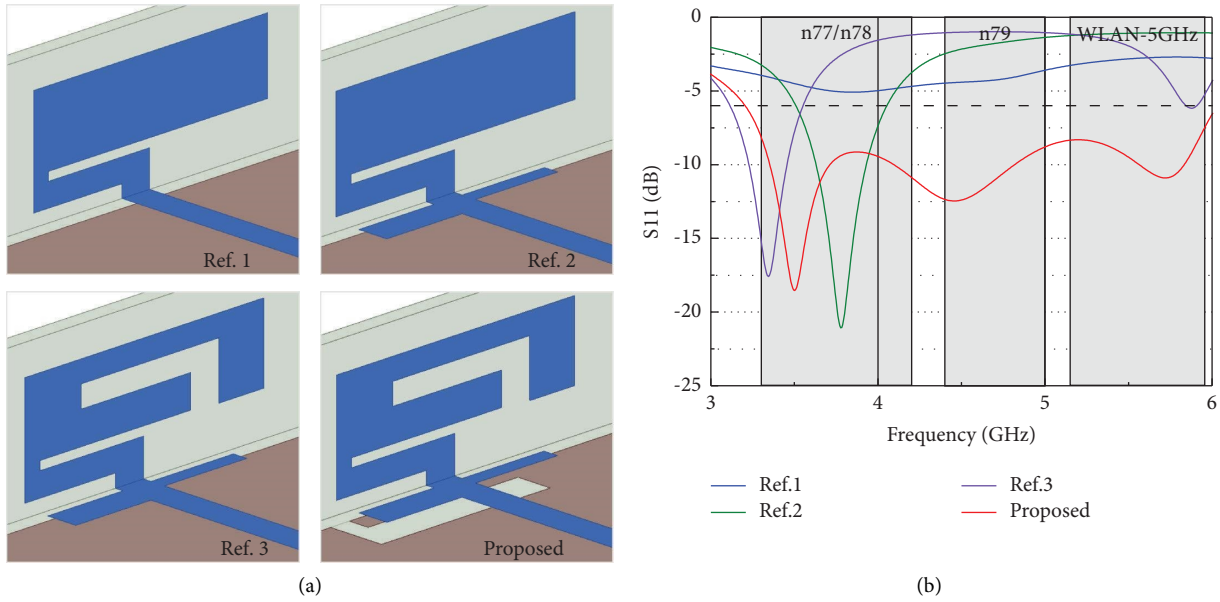

Figure 2: (a) The design steps and (b) its corresponding S parameters of the proposed antenna element.

Ref. 2. This introduces an additional resonant frequency at 5.9 GHz as the purple line in Figure 2(b). The resonant frequency at 3.8 GHz will shift to the lower frequency of approximately 3.4 GHz due to the lengthened electrical path caused by the inverted-L slot. Finally, the addition of an open slot on the ground plane forms the proposed antenna. An additional resonant frequency at 4.5 GHz is excited as the red line shown in Figure 2(b). The 6-dB impedance bandwidth of the proposed antenna is from 3200 to 6000 MHz and fully covers the required triple band.

To identify the excitation path of the resonant modes, the surface current distributions at 3.5, 4.5, and 5.7 GHz are shown in Figures 3 and 4. As shown in Figure 3(a), the current path ABCDEF (28.6 mm) of the dual-arm monopole structure excited at 3.5 GHz is approximately one-quarter wavelength long. However, the current distribution at 5.7 GHz consists of two current paths, as shown in Figure 3(b). The first one is the path ABCDFGH (28.6 mm) and two maximum currents with one current null can be observed on the path. The one-half-wavelength excitation can be inferred. The second one is the path ABCDE (19.1 mm), approximately one-quarter wavelength long. Because one maximum current on the path and a weak point at the end of the path can be observed. From the current path mentioned above, the resonant frequency at 3.5 GHz is generated by the longer arm of the dual-arm monopole structure. The resonant frequency at 5.7 GHz is collaboratively excited by the longer arm and the shorter arm of the dual-arm monopole structure. Next, the electric field and the current distribution of the open slot excited at 4.5 GHz are shown in Figures 4(a) and 4(b), respectively. There have some features that are worth mentioning. First, the direction of the electric field is perpendicular to the open slot path ABC, as shown in Figure 4(a). Second, the intensity of the electric field gradually decreases from the opening section to the closed section, and the current distribution gradually increases from the opening section to the closed section conversely, as shown in Figures 4(a) and 4(b). From those two features mentioned above, we can infer that the resonant frequency at 4.5 GHz is excited by the open slot on the ground plane.

2.3. Parametric Studies. To validate that the dual-arm monopole structure is responsible for the excitation of the resonant frequencies at 3.5 and 5.7 GHz and the open slot is responsible for the excitation of the resonant frequency at 4.5 GHz, parametric studies on L_1 (length of the longer arm), W_1 (width of the longer arm), L_2 (length of the shorter arm) and L_3 (length of the open slot) are investigated here. The corresponding location of the parameters is shown in Figure 5(a). Tuning L_1 will only affect the center frequency of the resonant frequency (f_1) at 3.5 GHz, which decreasing L_1 from 9.9 to 8.9 mm and the f_1 will shift from approximately 3.4 to 3.6 GHz, as shown in Figure 5(b). The optimum L_1 is chosen to be 9.4 mm because it can achieve a wide enough impedance bandwidth to cover the n77/78 bands and a good impedance matching (S_{11} reaches −15 dB) at the same time.

As shown in Figure 5(c), tuning W_1 will affect the f_1 and the resonant frequency (f_3) at 5.7 GHz simultaneously. When W_1 decreased from 1.5 to 0.5 mm, the f_1 and the f_3 will shift to the lower frequency without affecting the resonant frequency (f_2) at 4.5 GHz. The optimum W_1 is chosen to be 1 mm because the impedance bandwidth can fully cover the desired bands with the optimum performance both on bandwidth and impedance matching. If the W_1 is chosen to be 1.5 mm, then those resonant frequencies f_1 and f_3 are shifting to higher frequency but cannot cover the n77/78 bands.

Figure 5(d) shows that tuning L_2 will only affect the f_3 without affecting other resonant frequencies. When the L_2 increases from 5.3 to 6.1 mm, the resonant frequency f_3 will

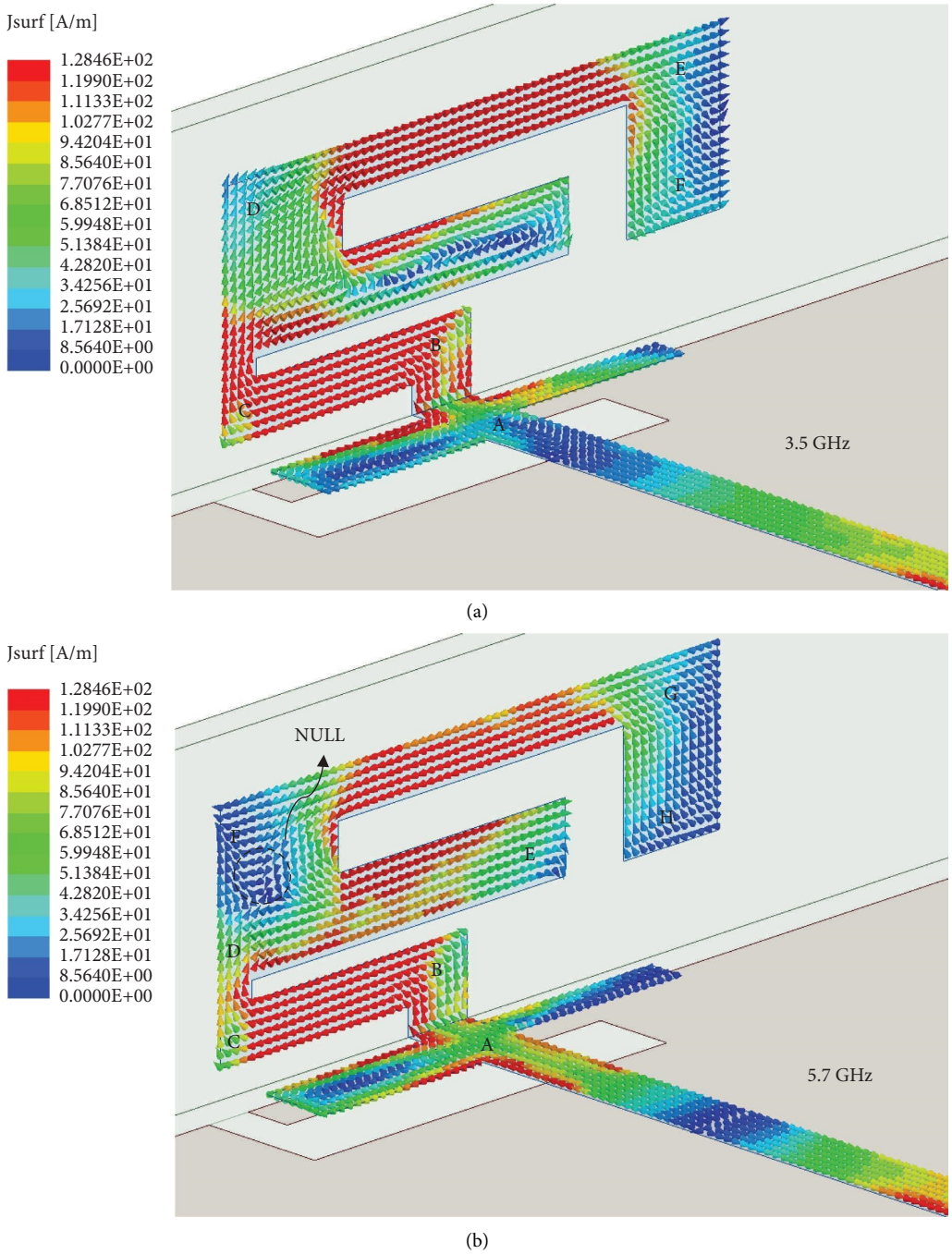

Figure 3: Current distributions of the dual-arm monopole structure at (a) 3.5 GHz and (b) 5.7 GHz.

shift from approximately 5.9 to 5.6 GHz. The optimum L_2 is chosen to be 5.8 mm because the bandwidth of the antenna is already wide enough to cover all the desired bands and it also shows that the proposed antenna has good frequency tunable performance.

From the studies mentioned above, we can verify that the f_1 is excited by the longer arm of the dual-arm monopole structure independently and the f_3 is excited by the longer arm and the shorter arm of the dual-arm monopole structure simultaneously. Finally, tuning L_3 will only affect the f_2 and without affecting those frequencies of the f_1 and f_3 as shown in Figure 5(e). When the L_3 increases from 8.5 to 9.5 mm, the f_2 will shift from approximately 4.6 to 4.2 GHz. The optimum L_3 is chosen to be 9 mm because there has the best reflection coefficient of these three results in all desired bands and 6-dB impedance bandwidth can

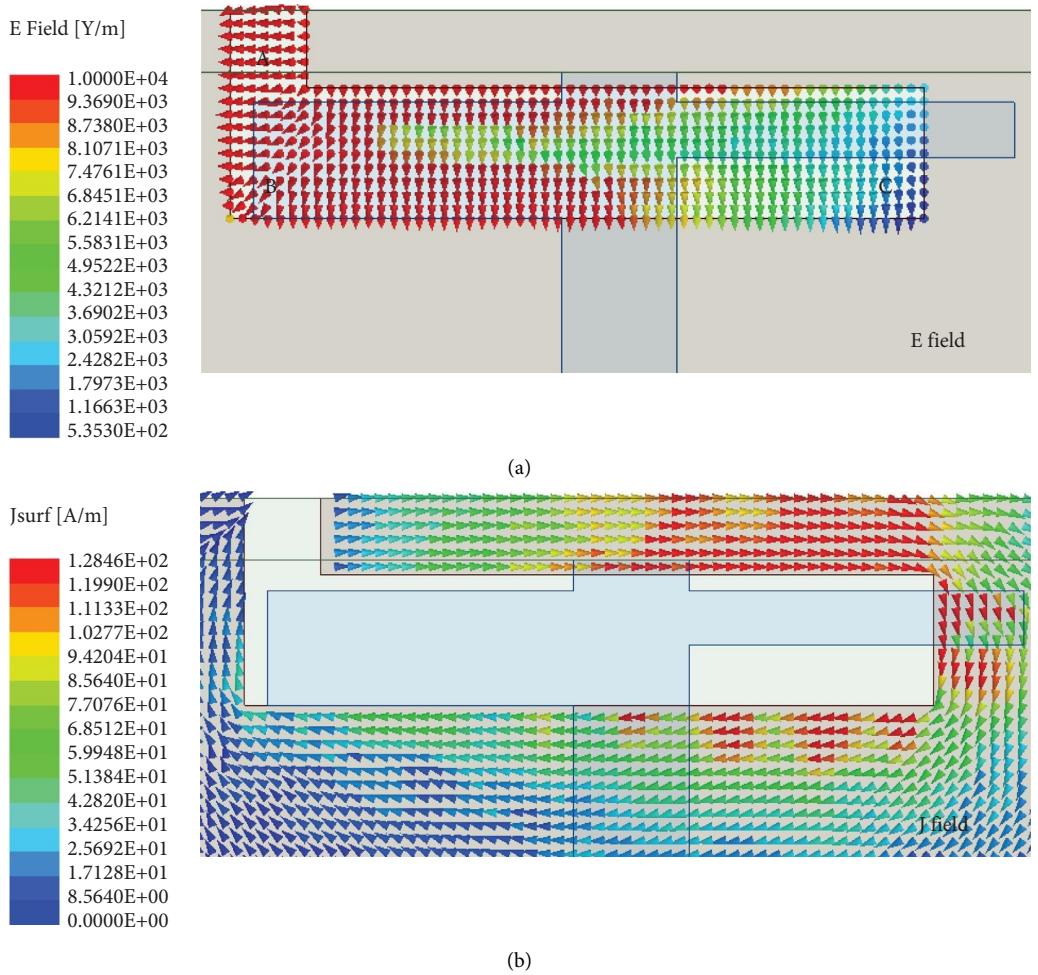

Figure 4: (a) The electric field intensity and (b) the current distribution of the open slot at 4.5 GHz.

fully cover the desired bands. Based on the result of the L_3, we can validate that the open slot is responsible for the f_2 independently.

3. Results and Discussion

The arrangement of the proposed eight-element antenna array is placed on the two side edges of the device as shown in Figure 6(a). The three-dimensional size of the device is $150 \times 75 \times 7.8\,mm^3$. In this case, Ant. 1–4 are the mirror of Ant. 5–8. Both the distances between Ant. 1 and Ant. 2, and between Ant. 3 and Ant. 4 are 29.8 mm. The distance between Ant. 2 and Ant. 3 is 30 mm. The photograph of the fabricated antenna array is shown in Figure 6(b). In this project, the simulations were performed by using Ansys HFSS.

The simulated and measured reflection coefficients and transmission coefficients of the proposed MIMO antenna array are shown in Figures 7 and 8, respectively. Good agreement between the simulated and measured results can be observed in these two figures. Figure 7 shows that the proposed MIMO antenna array has a wide 6-dB impedance bandwidth from approximately 3.2 to 6 GHz. The simulated transmission coefficients are all less than −12.6 dB across the desired bands, as shown in Figure 8. Furthermore, the measured results of the manufactured MIMO antenna array are also plotted in Figures 7 and 8. The measured results of the reflection coefficient validated that the proposed MIMO antenna array can cover the desired bands with a 6-dB impedance bandwidth of approximately 3.25 to over 6 GHz, and the transmission coefficients are all less than −10 dB without any isolation structure. The above results show that the proposed MIMO antenna array can support 5G smartphone applications in the 5G NR n77/n78/n79 and WLAN5-GHz bands.

The simulated and measured 2D radiation patterns of those Ant. 1–4 across different frequencies (3.7, 4.7, and 5.5 GHz) at the xy-plane are plotted in Figure 9. Because those Ant. 5–8 are symmetric to those Ant. 1–4, the radiation patterns of those Ant. 5–8 are not plotted, for brevity. One can see that the measured radiation patterns are highly consistent with the simulated results and each antenna has a unique radiation pattern with the orientation of the maximum gain pointing in different directions. However, the Ant. 1–4 at 4.7 and 5.5 GHz are mainly scattering toward the $-y$-direction and away from the system ground can be observed, which means that the antenna array has good MIMO performance and good isolation between the

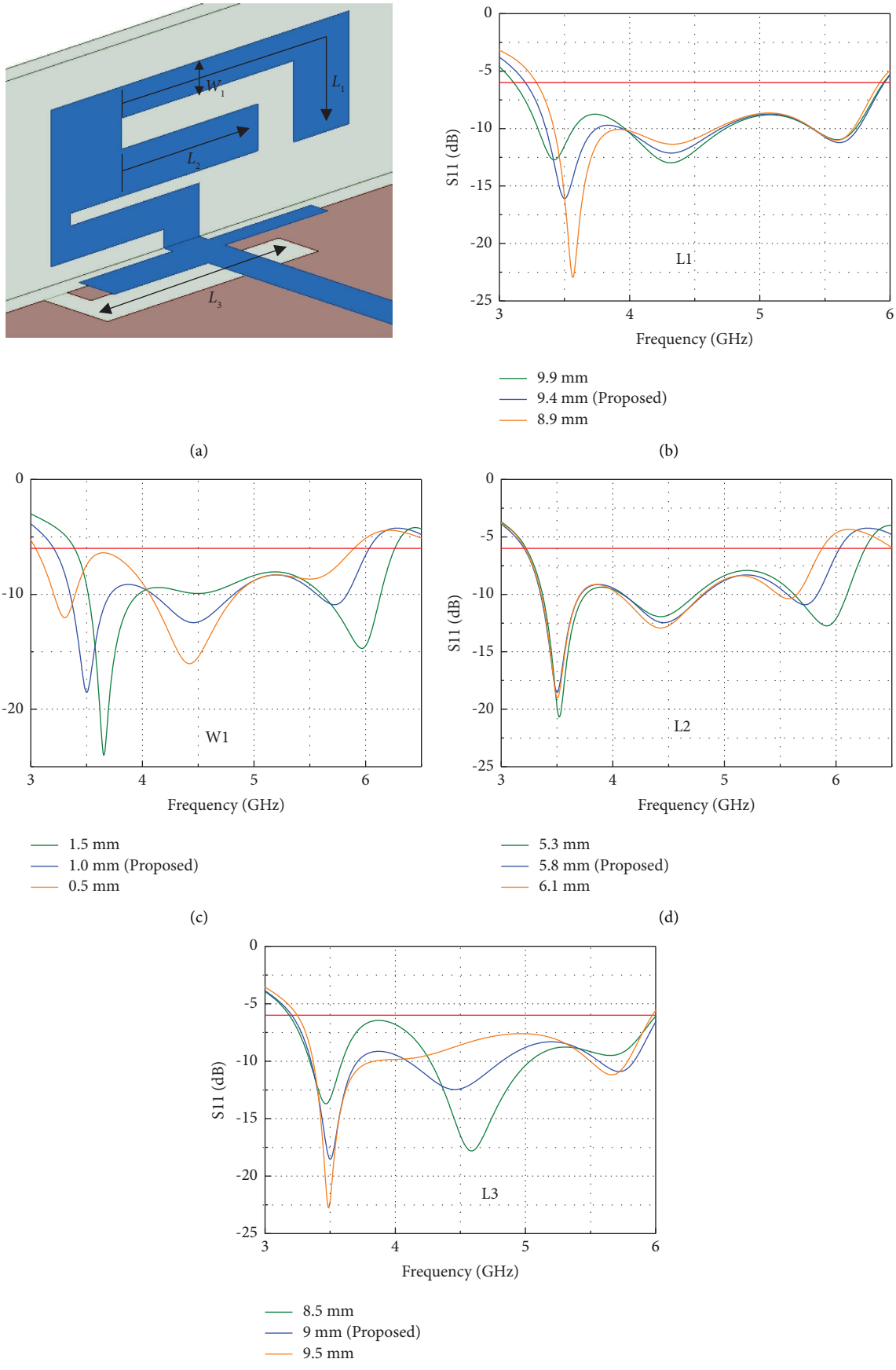

Figure 5: (a) Corresponding location of the parameters and the variety of the S parameter when tuning variables of (b) L_1, (c) W_1, (d) L_2, and (e) L_3.

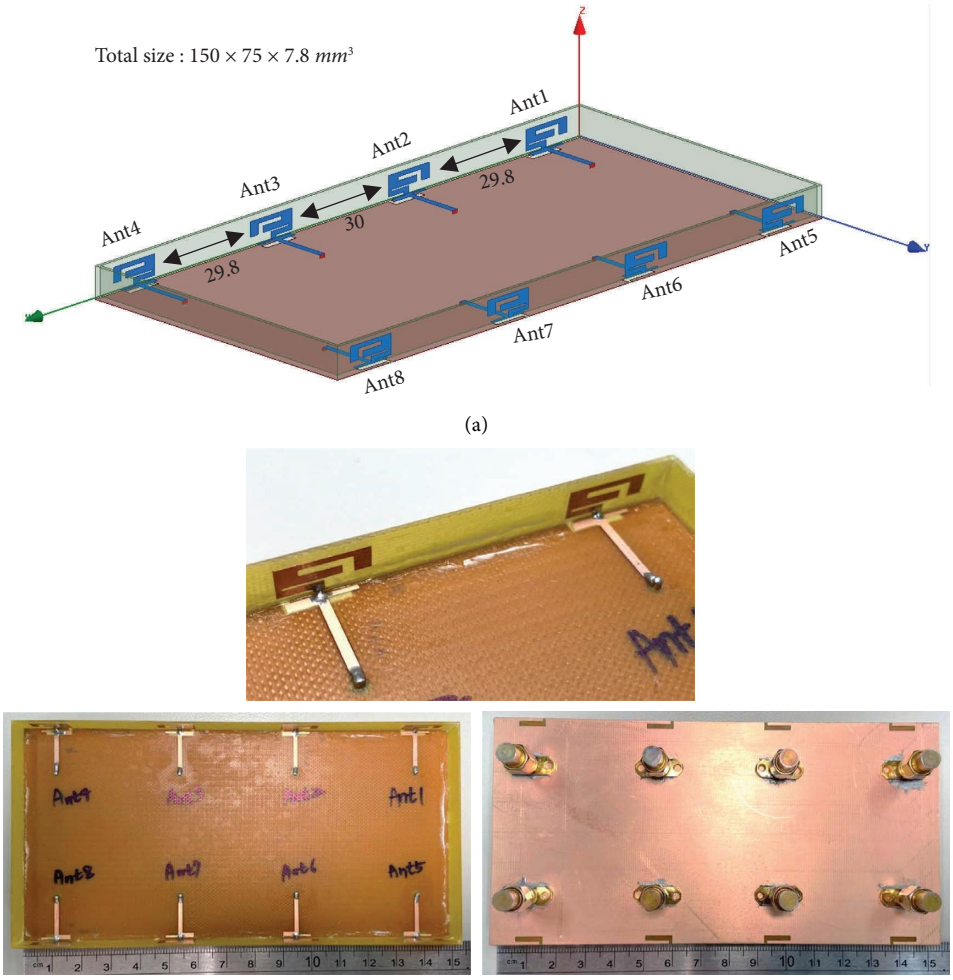

Figure 6: (a) The configuration of the MIMO antenna array and (b) the photograph of the fabricated MIMO antenna array.

opposite of the antennas at 4.7 and 5.5 GHz. Furthermore, the measured total efficiency of the proposed antenna ranges from 38% to 83% across the desired bands as shown in Figure 10.

To validate the MIMO performance of the proposed antenna array, the simulated ECCs and diversity gains are shown in Figure 11. The simulated ECCs of Ant. 1 and Ant. 2, Ant. 2 and Ant. 3, Ant. 1 and Ant. 5, and Ant. 2 and Ant. 6 are plotted in Figure 11(a). We chose these antenna pairs because they are the closest of the other antenna pairs and because of the symmetrical structure, the other antenna pairs are not included for brevity. The results of simulated ECCs show that most of those antenna pairs have ECC values less than 0.1 except the antenna pair of Ant. 1 and Ant. 5, but overall the ECCs of the proposed MIMO antenna array can still achieve less than 0.31 across the desired bands. The diversity gains [17, 18] of the proposed antenna array are shown in Figure 11(b) and for brevity, only a relatively close antenna pair has been plotted. According to industry standards, the DG values should be kept around 10 dB. One can see that all the values in the required bands are lies around the 10 dB line, except the result of Ant.1 and Ant. 5 at around 3.4 GHz is slightly deviating from the 10 dB line due to the isolation a little bit lower than the others and relatively high ECC value.

To validate the performance of the proposed antenna array, Table 1 shows the comparison of the performance between the antennas in the previously published literature and the proposed one. Here, the proposed antenna shows a very wide operating bandwidth from 3.3 to 6 GHz that can cover the 5G NR n77/78/79 and WLAN-5GHz bands. Moreover, the isolation and efficiency are also comparable to the references. The isolation of the proposed antenna array can reach 12.6 dB without any decoupling element and the efficiency can reach up to 83%. Even though the proposed antenna may have shown a slightly higher ECC value than the other references, but it just happens in the antenna pair of Ant. 1 and Ant. 5 in the frequency range of 3.3 to 3.5 GHz. In conclusion, the proposed antenna array has superior bandwidth performance compared to the other references.

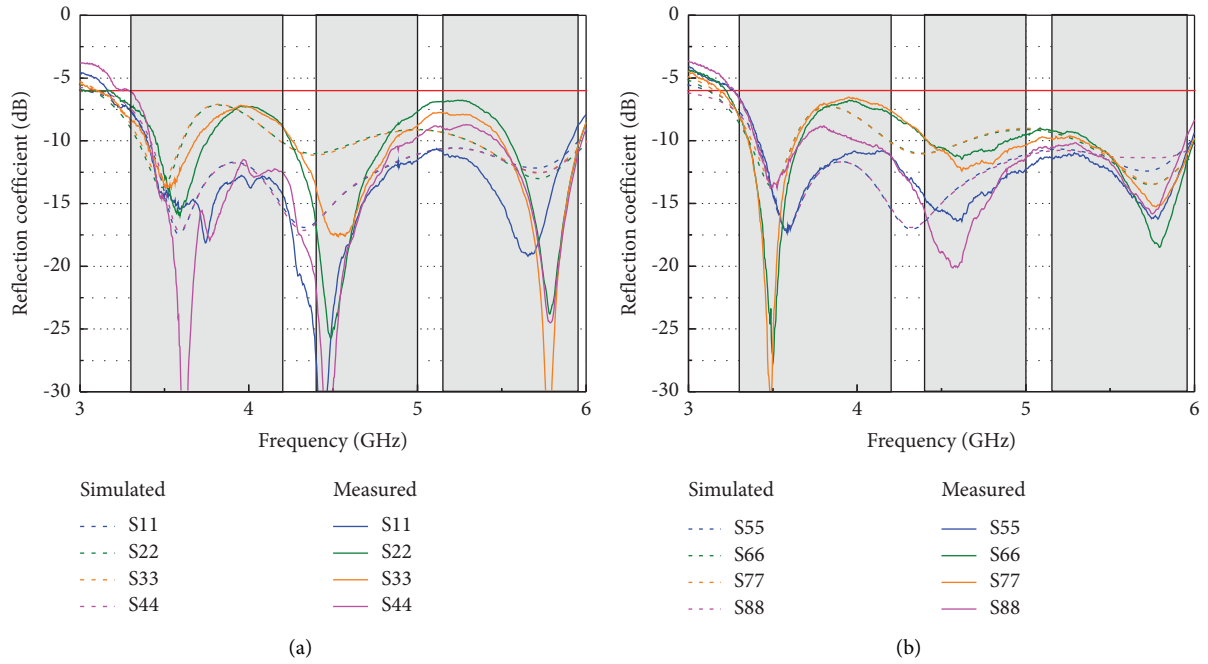

Figure 7: Simulated and measured reflection coefficients of the (a) antenna 1 to antenna 4 and (b) antenna 5 to antenna 8.

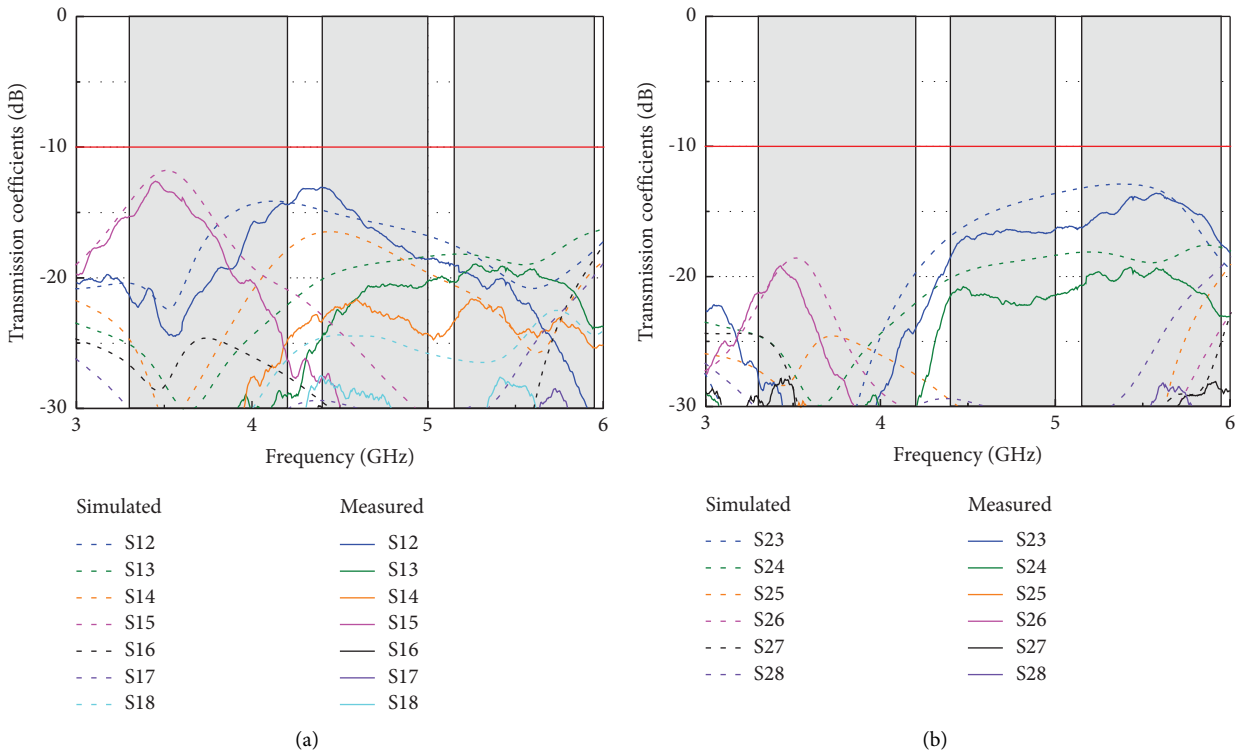

Figure 8: Simulated and measured transmission coefficients (a) between antenna 1 and the other antennas and (b) between antenna 2 and the other antennas.

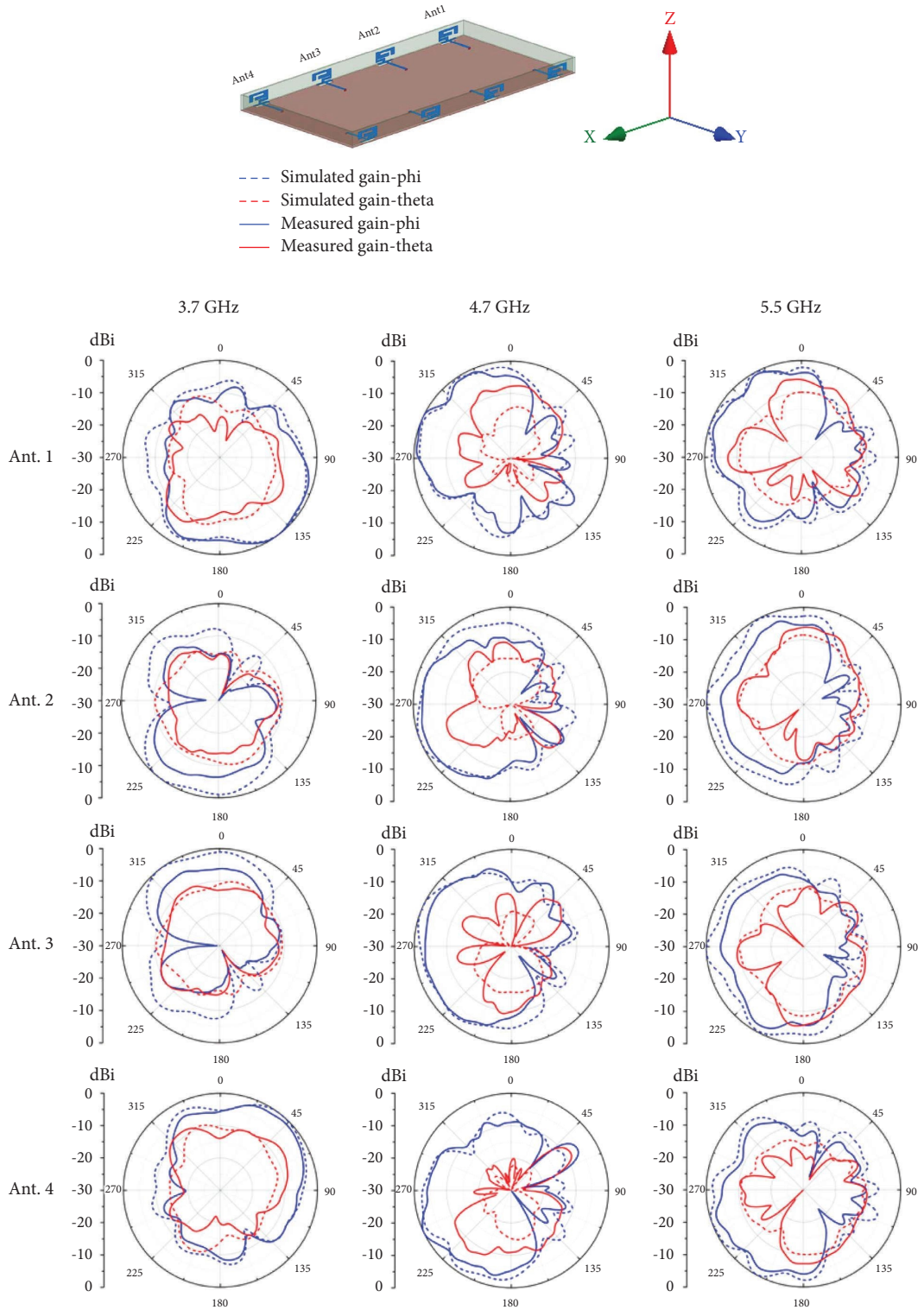

Figure 9: Simulated and measured 2D radiation patterns of Ant. 1–4 at the xy-plane in 3.7, 4.7, and 5.5 GHz.

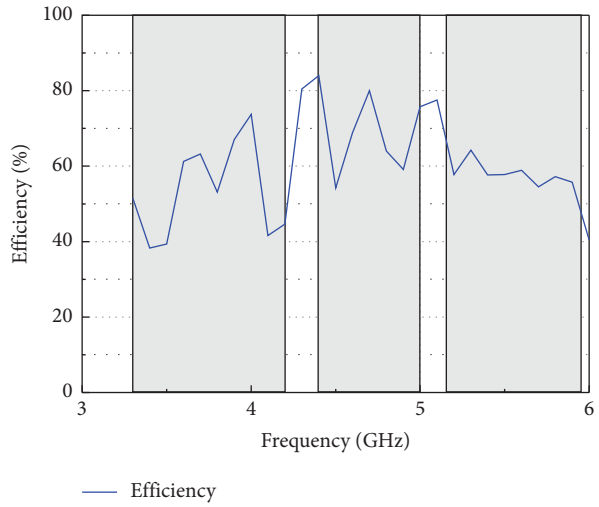

Figure 10: Measured antenna total efficiency.

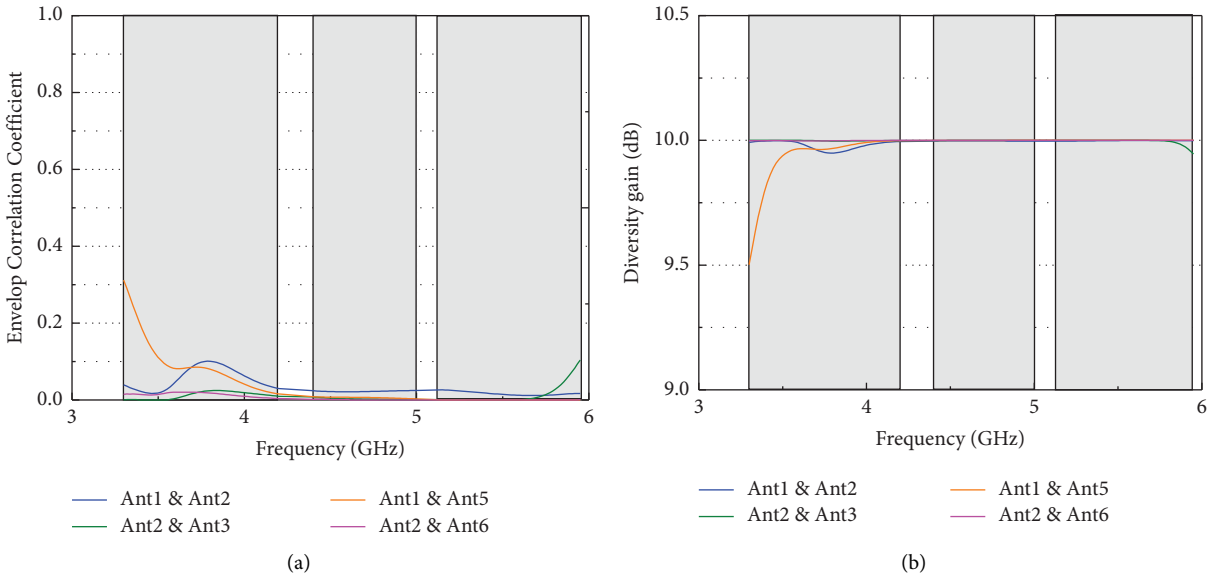

Figure 11: (a) Simulated ECCs and (b) diversity gains.

Table 1: Comparison with previously published literature.

Ref.	Bandwidth (6-dB/GHz)	Decoupling element	Efficiency (%)	Isolation (dB)	MIMO order	ECC
[1]	3.3–3.8, 4.8–5.0, 5.15–5.925	No	43–73	>10.5	8	<0.12
[2]	3.4–3.6, 5.725–5.825 (10-dB)	No	41–59	>10	12	<0.2
[3]	3.4–3.6 (10-dB)	No	40–52	>10	8	<0.15
[5]	3.3–5.8 (10-dB)	No	55–87	>15	4	<0.03
[6]	3.3–5.0	No	46–76	>14.5	8	<0.1
[7]	3.3–7.1	No	47–70	>11	8	<0.09
[8]	3.25–5.93 (10-dB)	No	41–69	>10	8	<0.1
[9]	3.3–3.6, 4.8–5.0	Yes	45–78	>12	10	<0.15
[10]	3.3–3.6	Yes	45–60	>15	8	<0.15
[11]	3.4–3.6, 4.8–5.1	Yes	41–72	>11.5	8	<0.08
[12]	3.4–3.6	No	60–68	>19.1	8	<0.0125
[13]	3.4–3.6	No	38–64	>12.7	4	<0.13
[14]	3.38–3.82, 4.8–5.6	Yes	40–85	>15.5	8	<0.07
[15]	3.3–6.0	Yes	40–90	>18	8	<0.05
[16]	3.3–7.5	No	40–78	>10	4	<0.05
Pro.	**3.3–6.0**	**No**	**38–83**	**>12.6**	**8**	**<0.31 (Ant. 1 and 5) <0.1 (others)**

4. Conclusions

A wideband and simple structure MIMO antenna array for 5G smartphone application is presented in this paper. The proposed MIMO antenna array fully covers the entire 5G NR n77/n78/n79 and WLAN-5GHz bands with a 6-dB impedance bandwidth range from 3.2 to 6 GHz, and the isolations are all more than 10 dB without any isolation structure or techniques. To validate the design concept, the proposed MIMO antenna array was fabricated and measured. Good agreement of the reflection coefficients, the isolations, and the 2D radiation patterns are obtained between the simulated and measured results. Furthermore, the total efficiency of the antenna ranges from 38 to 83%. The simulated ECCs are all less than 0.31. Therefore, the above experimental results validate that the proposed MIMO antenna array can support 5G smartphone applications.

Data Availability

The data used to support the findings of this study are included within the article.

Conflicts of Interest

The authors declare that there are no conflicts of interest regarding the publication of this paper.

Acknowledgments

The authors would like to thank the Ministry of Science and Technology (Taiwan) and National Pingtung University for partially sponsoring this work (MOST 106-2633-E-153 -001-).

References

[1] H. Wang, R. Zhang, Y. Luo, and G. Yang, "Compact eight-element antenna array for triple-band MIMO operation in 5G mobile terminals," *IEEE Access*, vol. 8, pp. 19433–19449, 2020.

[2] Z. Tian, R. Chen, and C. Li, "Dual-band inverted F-shaped antenna array for sub-6 GHz smartphones," in *Proceedings of the 2019 IEEE 89th Vehicular Technology Conference (VTC2019-Spring)*, pp. 1–5, Kuala Lumpur, Malaysia, April 2019.

[3] K. L. Wong, C. Y. Tsai, and J. Y. Lu, "Two asymmetrically mirrored gap-coupled loop antennas as a compact building block for eight-antenna MIMO array in the future smartphone," *IEEE Transactions on Antennas and Propagation*, vol. 65, no. 4, pp. 1765–1778, 2017.

[4] H. Wang and G. Yang, "Wideband Antenna system for multi-band 8×8 MIMO operation in the 5G mobile terminals," in *Proceedings of the 2019 International Symposium on Antennas and Propagation (ISAP)*, pp. 1–3, Xi'an, China, October 2019.

[5] Z. Zheng, J. D. Ntawangaheza, and L. Sun, "Wideband MIMO antenna system for sub-6 GHz cell phone," in *Proceedings of the 2021 International Conference on Electronics, Circuits and Information Engineering (ECIE)*, pp. 1–5, Zhengzhou, China, January 2021.

[6] A. Zhao and Z. Ren, "Wideband MIMO antenna systems based on coupled-loop antenna for 5G N77/N78/N79 applications in mobile terminals," *IEEE Access*, vol. 7, pp. 93761–93771, 2019.

[7] Q. Cai, Y. Li, X. Zhang, and W. Shen, "Wideband MIMO antenna array covering 3.3–7.1 GHz for 5G metal-rimmed smartphone applications," *IEEE Access*, vol. 7, pp. 142070–142084, 2019.

[8] C.-Y.-D. Sim, H.-Y. Liu, and C.-J. Huang, "Wideband MIMO antenna array design for future mobile devices operating in the 5G NR frequency bands n77/n78/n79 and LTE band 46," *IEEE Antennas and Wireless Propagation Letters*, vol. 19, no. 1, pp. 74–78, 2020.

[9] W. Hu, X. Liu, S. Gao et al., "Dual-band ten-element MIMO array based on dual-mode IFAs for 5G terminal applications," *IEEE Access*, vol. 7, pp. 178476–178485, 2019.

[10] W. Jiang, B. Liu, Y. Cui, and W. Hu, "High-isolation eight-element MIMO array for 5G smartphone applications," *IEEE Access*, vol. 7, pp. 34104–34112, 2019.

[11] J. Guo, L. Cui, C. Li, and B. Sun, "Side-edge frame printed eight-port dual-band antenna array for 5G smartphone applications," *IEEE Transactions on Antennas and Propagation*, vol. 66, no. 12, pp. 7412–7417, 2018.

[12] A. Zhao and Z. Ren, "Size reduction of self-isolated MIMO antenna system for 5G mobile phone applications," *IEEE Antennas and Wireless Propagation Letters*, vol. 18, no. 1, pp. 152–156, 2019.

[13] L. Chang, Y. Yu, K. Wei, and H. Wang, "Polarization-orthogonal Co-frequency dual antenna pair suitable for 5G MIMO smartphone with metallic bezels," *IEEE Transactions on Antennas and Propagation*, vol. 67, no. 8, pp. 5212–5220, 2019.

[14] W. Hu, L. Qian, S. Gao et al., "Dual-band eight-element MIMO array using multi-slot decoupling technique for 5G terminals," *IEEE Access*, vol. 7, pp. 153910–153920, 2019.

[15] X.-T. Yuan, W. He, K.-D. Hong, C.-Z. Han, Z. Chen, and T. Yuan, "Ultra-wideband MIMO antenna system with high element-isolation for 5G smartphone application," *IEEE Access*, vol. 8, pp. 56281–56289, 2020.

[16] X.-T. Yuan, Z. Chen, T. Gu, and T. Yuan, "A wideband PIFA-pair-based MIMO antenna for 5G smartphones," *IEEE Antennas and Wireless Propagation Letters*, vol. 20, no. 3, pp. 371–375, 2021.

[17] J. Kulkarni, A. G. Alharbi, A. Desai, C.-Y.-D. Sim, and A. Poddar, "Design and analysis of wideband flexible self-isolating MIMO antennas for sub-6 GHz 5G and WLAN smartphone terminals," *Electronics*, vol. 10, no. 23, p. 3031, 2021.

[18] J. Kulkarni, S. Dhabre, S. Kulkarni, C.-Y. D. Sim, R. K. Gangwar, and K. Cengiz, "Six-Port symmetrical CPW-fed MIMO antenna for futuristic smartphone devices," in *Proceedings of the 2021 6th International Conference for Convergence in Technology (I2CT)*, pp. 1–5, Pune, India, April 2021.